17th World Conference on Earthquake Engineering, 17WCEE
Sendai, Japan - September 13th to 18th 2020

Development of a New Type of Damage-Visible Shear Buckling-Restrained Braces

Liang-Jiu Jia[(1)], Jiang-Yue Xie[(2)], Zeqing Wang[(3)], Kana Kondo[(3)], and Hanbin Ge[(4)]

[(1)] *Associate Professor, College of Civil Engineering, Tongji University, Shanghai, China, lj_jia@tongji.edu.cn*

[(2)] *Graduate Student, College of Civil Engineering, Tongji University, Shanghai, China, 1832340@tongji.edu.cn*

[(3)] *Graduate Student, Department of Civil Engineering, Meijo University, Shiogamaguchi, Japan*

[(4)] *Professor, Department of Civil Engineering, Meijo University, Shiogamaguchi, Japan, gehanbin@meijo-u.ac.jp*

Abstract

This paper proposes a buckling-restrained brace made of a core plate with shear fuses connected in series (hereafter termed as SBRBs). The SBRB consists of a core plate, two filling plates, two perforated cover plates, unbounding material and bolts. It is designed to dissipate seismic energy via yielding mainly under shear. The perforated cover plates make damage of the core plate visible. To analyze the SBRBs, seven specimens were designed with different number of shear fuses, tension-to-shear strength ratios and radii of shear fuses. The applied loading history was cyclic incremental loading. Analytical models were proposed, and formulae to evaluate the initial stiffness and yield strength of the SBRBs were derived based on the principle of virtual work. In addition, finite element analyses of the specimens were carried out. In the experiments, it was found that the deformation capacity had positive correlation with the number of the shear fuses, tension-to-shear strength ratio, and radii of shear fuses. Fracture modes of all the specimens were shear rupture, and excellent ductility and energy dissipation capacity were obtained. The analytical results were in good agreement with the experimental ones. Contact between the core plate and the filling plates due to flexural deformation was successfully simulated by the numerical study.

Keywords: Shear buckling-restrained brace, Metallic damper, Cyclic loading, Seismic, Damage-visible, All-steel

1. Introduction

Buckling-restrained braces (BRBs) are widely employed in earthquake resistant structures because of their high stiffness, limited structural and non-structural damage and possibility of replacement after a severe seismic event [1-4]. A conventional BRB consists of a metallic core that can yield under tension and compression. The core is restrained against buckling by a casing, and a gap is generally set between the core plate and the casing [5-7]. Some researchers have developed a BRB with a core plate that does not change significantly in cross-sectional area under loading. These BRBs have good hysteretic behaviors and are easily inspectable [8, 9]. However, they may be susceptible to ultra-low-cycle fatigue due to the shape of the holes within the core plate, which limits their cumulative deformation capacity.

Seismic performance of BRBs can be improved by changing the stress states of the cores. Some researchers proposed BRBs with perforated metallic cores, such as steel slit configuration, which dissipate energy not only by axial plastic deformation, but also by shear and bending deformation [10-14]. They were proved to be effective in energy dissipation and damage reduction [15]. Benavent-Climent proposed a new brace-type seismic damper, which consists of a tube-in-tube assemblage of two hollow structural sections. The experimental results showed that the damper has stable hysteretic characteristics and excellent axial-shear-bending energy dissipation capacity [16]. The authors [17] showed that the perforated configuration under shear dominant loading leaded to stable and symmetric hysteretic curves.

Based on these characteristics, a buckling-restrained brace made of a core plate with shear fuses connected in series (hereafter termed as SBRB) as shown in Fig. 1 were proposed in this study. Compared with slit dampers and shear panel dampers commonly with two additional strong bracings, no additional steel bracings are required for the proposed SBRBs, which can thus reduce cost. The core plate of an SBRB consists of shear fuses connected in series as shown in Fig. 2 to increase deformation capacity. To prevent the core plate from buckling, cover plates, filling plates and unbounding material are employed to restrain the core plate. In addition, perforated cover plates make damage to the core plate visible, leading to convenient inspection.

2. Experimental Program

2.1 Specimens design

The proposed SBRB is a type of all-steel BRB, which is made of SS400 with a nominal yield stress of 235 MPa. The configuration and the size of the specimens is illustrated in Fig. 1 and Table 1. The in-plane (strong axis) gap between the core plate and the filling plates is 1 mm. This kind of SBRB is expected to replace shear dampers but not conventional BRBs. Yielding first occurs at these locations and shear deformation mainly occurs in these shear fuses, which leads to stable hysteretic behaviors.

A mechanical model of the shear fuse can be established in Fig. 3. The tensile yield strength of the shear fuse and the ultimate shear strength are defined as T_y and Q_u respectively. The tension-to-shear strength ratio, U, is defined in Eq. (1),

$$U = T_y / Q_u \tag{1}$$

The desired failure mode is shear failure of the shear fuse, which is affected by U. So $U > 1.7$. Likewise, the radius, R and number of the shear fuses, N can also have a significant effect on seismic performance. Detailed parameters of the tested specimens are shown in Table 1.

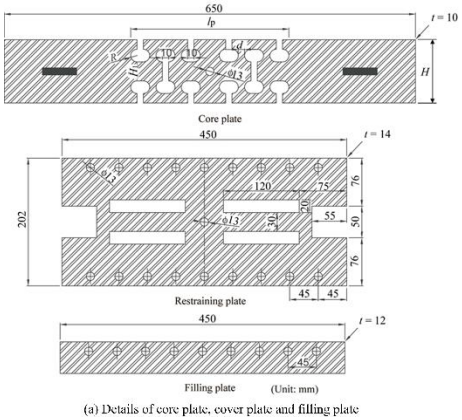

(a) Details of core plate, cover plate and filling plate

Fig. 1 – Details of core plate, cover plate and filling plate

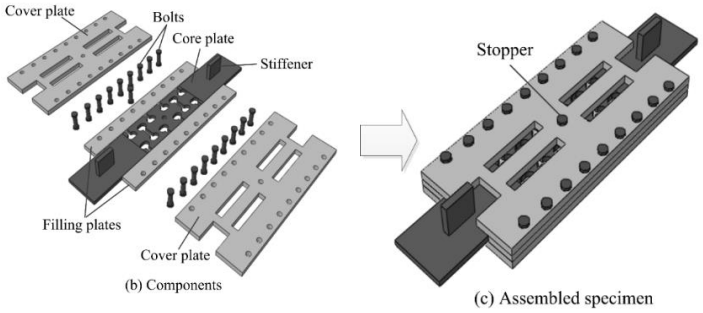

Fig. 2 – Components of an SBRB

Table 1 – Parameters of SBRB specimens

No.	Specimen	N	U	R (mm)	l_p (mm)	H (mm)	A_S (mm^2)	A_N (mm^2)
1	SBRB-N2U2.6R10	2	2.6	10	170	100	200	300
2	SBRB-N4U2.6R10	4	2.6	10	250	100	200	300
3	SBRB-N6U2.6R10	6	2.6	10	330	100	200	300
4	SBRB-N4U1.7R10	4	1.7	10	250	80	200	200
5	SBRB-N4U1.0R10	4	1.0	10	250	64	200	120
6	SBRB-N4U2.6R15	4	2.6	15	310	120	200	300
7	SBRB-N4U2.6R20	4	2.6	20	370	140	200	300

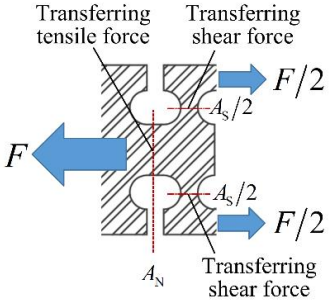

Fig. 3 – Mechanical model of shear fuses

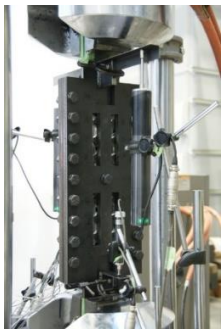

Fig. 4 – Test setup

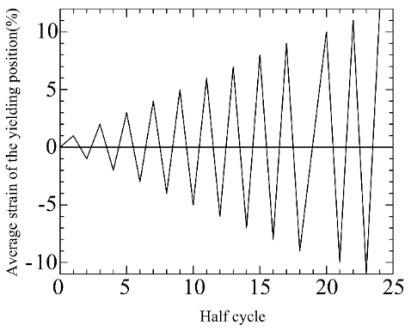

Fig. 5 – Loading history

2.2 Test setup and loading history

As shown in Fig. 4, the experiments were conducted using an MTS testing system. One end of the specimen is fixed, while the longitudinal freedom of the other end is free. The loading history is shown in Fig. 5.

3. Experiment Result

3.1 Effect of number of shear fuses

In these tests, force-displacement results of Specimens SBRB-N2U2.6R10, N4U2.6R10 and SBRB-N6U2.6R10 are shown in Table 2 and Fig. 6. In addition, apparent increase of the stress can be observed at

large strain ranges, which is mainly for the contact between the core plate and the filling plates.

Table 2 – Effect of number of shear fuses

No.	Specimen	*N*	T_y (kN)	Q_u (kN)	Half cycle (crack initiation)	Half cycle (contact)	Half cycle (rupture)	Failure mode
1	SBRB-**N2**U2.6R10	2	81.8	31.5	4	-	9	Shear failure
2	SBRB-**N4**U2.6R10	4	81.8	31.5	8	8	13	
3	SBRB-**N6**U2.6R10	6	81.8	31.5	6	8	12	

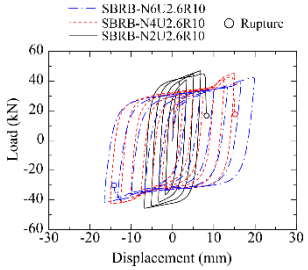

Fig. 6 – Effect of *N*

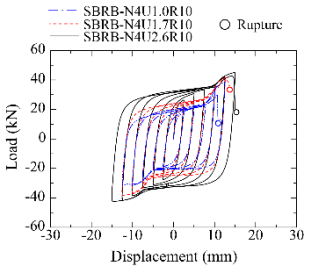

Fig. 7 – Effect of *U*

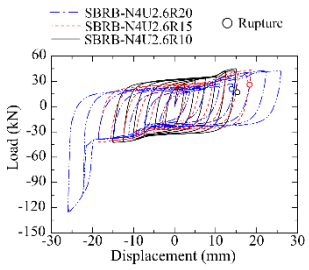

Fig. 8 – Effect of *R*

3.2 Effect of tension-to-shear strength ratio

The tension-to-shear strength ratio *U* represents proportion of shear force and tensile force. The results are shown in Table 3 and Fig. 7. Excessive bending deformation can lead to premature failure of the core plate, causing deformation capacity increases with an increasing *U* for the three specimens.

Table 3 – Effect of tension-to-shear strength ratio

No.	Specimen	*U*	T_y (kN)	Q_u (kN)	Half cycle (crack initiation)	Half cycle (contact)	Half cycle rupture)	Failure mode
2	SBRB-N4**U2.6**R10	2.6	81.8	31.5	8	8	13	Shear failure
4	SBRB-N4**U1.7**R10	1.7	54.5	31.5	4	6	11	
5	SBRB-N4**U1.0**R10	1.0	32.7	31.5	2	6	11	

3.3 Effect of radius of shear fuse

The radius of the shear fuse has a significant effect on ductility and cracking of the specimens, which are shown in Table 4 and Fig. 8. The ultimate strength of the three specimens before the contact of two neighboring shear fuses nearly stays the same and the failure mode of the three specimens is still shear failure, which is shown in Figs. 9 and 10.

Table – 4 Effect of radius of shear fuse

No.	Specimen	*R* (mm)	T_y (kN)	Q_u (kN)	Half cycle (crack nitiation)	Half cycle (contact)	Half cycle (rupture)	Failure mode
2	SBRB-N4U2.6**R10**	10	81.8	31.5	8	8	13	Shear failure
6	SBRB-N4U2.6**R15**	15	81.8	31.5	8	5	13	
7	SBRB-N4U2.6**R20**	20	81.8	31.5	12	3	15	

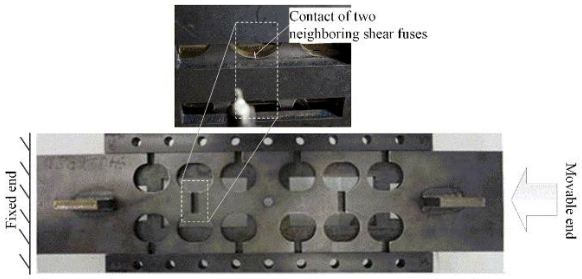

Fig. 9 – Contact of two neighboring shear fuses in SBRB-N4U2.6R20

Fig. 10 – Cracking process of Specimen SBRB-N6U2.6R10

4. Theoretical analysis

Mechanical behaviors of the proposed SBRB depend on the properties of the shear fuses. Main mechanical parameters of an SBRB are the initial stiffness, yield strength and ultimate strength. To determine these parameters, the internal force of an SBRB was analyzed based on the Principle of Virtual Work and Force Method. There 2 different kinds of shear fuses are defined as shown in Fig. 11, i.e., middle shear fuse and end shear fuse.

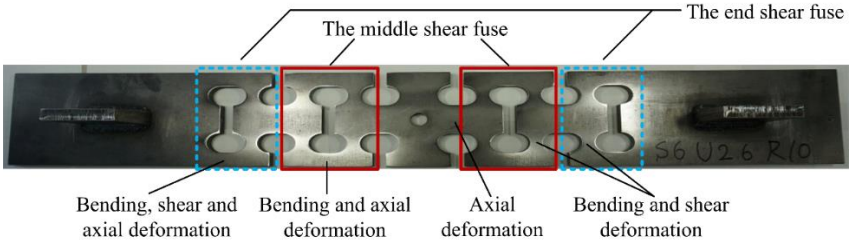

Fig. 11 – Two different types of shear fuses

4.1 Initial Stiffness of SBRB

An SBRB consists of few shear fuses in series. The initial stiffness can be obtained by analyzing the deformation of SBRB subjected to an applied load *F*.

The middle shear fuse is symmetric, and a simplified mechanical model of the middle shear fuse is presented in Fig. 12. Using the Principle of Virtual Work, equivalent widths of uniform cross sections can be obtained. The deformation of the specimens with middle shear fuse is given in Eqns. (2) to (4),

$$\Delta_M = \frac{12k_0FRd\left(B_1+2R\right)}{EtB_1^3}\left[1+\frac{2R}{d}\left(\frac{B_1}{B_1+k_3R}\right)^3\right]+\frac{16FR^3\left(3k_0^2-6k_0+4\right)}{Et\left(B-2k_1R\right)^3} \quad (2)$$

$$\Delta_S = \frac{9.6FR\left(1+\nu\right)}{Et\left(B-2k_2R\right)} \quad (3)$$

$$\Delta_N = \frac{Fd}{Et}\left(\frac{1}{B_1}+\frac{1}{B_1+R}+\frac{2R}{d}\left(\frac{1}{B_1+k_4R}\right)+4\left(1+\frac{R}{d}\right)\frac{1}{H_1}\right) \quad (4)$$

where Δ_M, Δ_S, Δ_N are bending, shear and axial deformation, respectively. k_3 and k_4 are the coefficients related to the widths of the equivalent uniform cross section models. t is the thickness of the core plate. v is the Passion's ratio of the steel. d, R, B, B_1 and H_1 are size parameters of the shear fuses as shown in Fig. 12(a).

Likewise, deformation of the end shear fuse can be obtained by the same method. All of the results are shown in Table 5 and errors are below 11%.

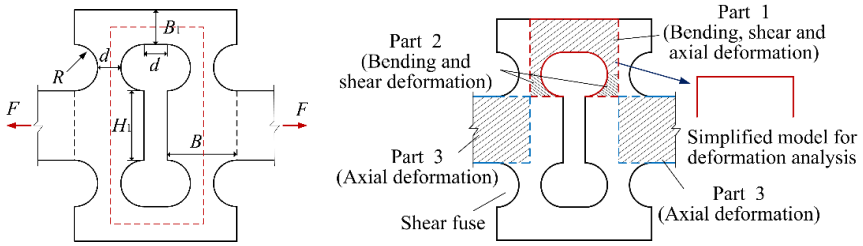

(a) Simplified model for middle shear fuse

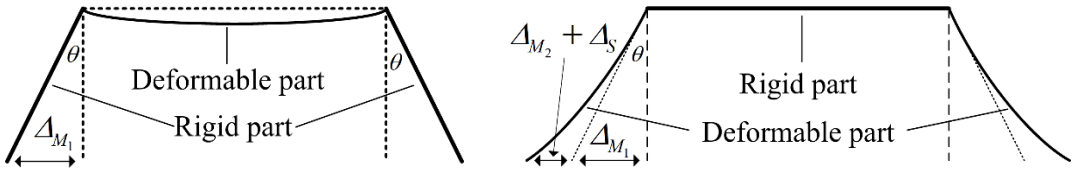

(b) Bending deformation of longitudinal part

(c) Bending and shear deformation of lateral part

Fig. 12 – Analytical model for bending and shear deformation of middle shear fuse

Table 5 – Theoretical and experimental initial stiffness of SBRBs

No.	Specimens	Experiment (kN/mm)	Theory (kN/mm)	Relative error (%)
1	SBRB-N2U2.6R10	80.7	85.4	5.82
2	SBRB-N4U2.6R10	37.0	40.6	9.73
3	SBRB-N6U2.6R10	31.0	27.6	11.00
4	SBRB-N4U1.7R10	30.0	32.7	9.00
5	SBRB-N4U1.0R10	24.5	25.8	5.31
6	SBRB-N4U2.6R15	24.2	26.7	10.30
7	SBRB-N4U2.6R20	15.9	16.3	2.52

4.2 Yield strength and ultimate strength of SBRB

Based on the analytical analysis and experimental results, yield strength and of the SBRBs is the minimum value among Eqns. (5) to (7), which shown the yielding in lateral part, longitudinal part of the shear fuse.

$$F_y \le \frac{4}{3}dt\tau_y \quad (5)$$

$$F_y \le \frac{2\sigma_y}{\frac{1}{B_1 t}+\frac{6k_0 r}{B_1^2 t}} \quad (6)$$

$$F_y \le \frac{2B_1 d}{9}\left(\frac{3d}{r}+4\right)\tau_y \quad (7)$$

where σ_y and τ_y are the yield normal stress and the yield shear stress, respectively.

According to the experimental results, the failure modes of all the specimens are ductile shear failure. Therefore, the ultimate strength can be expressed by Eq. (8),

$$F_u \le 2dt\tau_u \tag{8}$$

where τ_u is the ultimate shear stress of the material. The theoretical and experimental results are compared in Table 6.

Table 6 – Comparison of theoretical and experimental strength of SBRBs

No.	Specimen	$Q_{y,exp}$ (kN)	$Q_{y,theor}$ (kN)	$Q_{y,theor}/Q_{y,exp}$	$Q_{u,exp}$ (kN)	$Q_{u,theor}$ (kN)	$Q_{u,theor}/Q_{u,exp}$
1	SBRB-N2U2.6R10	20.26	20.98	1.03	46.9	48.7	1.04
2	SBRB-N4U2.6R10	16.88	16.35	0.97	45.2	48.7	1.08
3	SBRB-N6U2.6R10	16.20	16.35	1.01	42.5	48.7	1.15
4	SBRB-N4U1.7R10	11.88	9.91	0.83	41.6	48.7	1.17
5	SBRB-N4U1.0R10	11.47	9.34	0.81	38.4	48.7	1.26
6	SBRB-N4U2.6R15	12.86	11.68	0.91	43.6	48.7	1.12
7	SBRB-N4U2.6R20	10.45	9.08	0.87	42.8	48.7	1.14
Average				0.92			1.14
CoV				0.095			0.061

5. Finite element analysis

All specimens were analyzed using finite element (FE) software ABAQUS. Three-dimensional numerical model of the SBRB was established with solid elements C3D8R. The combined hardening model was employed, and self-contact and contact between the core plate, the filling plates and cover plates was simulated with the Coulomb friction model with a frictional coefficient of 0.2. Fig. 13 shows comparison results between the numerical simulation and the experiments. Increase in the load due to contact between the filling plates and the core plate was successfully simulated by the numerical simulation. Numerical and experimental results were listed in Table 7. The deviations only range from about 0.5 to 1.5 cycles.

Table 7 – Half cycle number of contact of test and FE results

No.	Specimen	Half cycle number when filling plates contact with core plate	
		Experiment	Simulation
1	SBRB-N2U2.6R10	-	7
2	SBRB-N4U2.6R10	8	7
3	SBRB-N6U2.6R10	8	5
4	SBRB-N4U1.7R10	6	5
5	SBRB-N4U1.0R10	6	4
6	SBRB-N4U2.6R15	6	5
7	SBRB-N4U2.6R20	5	3

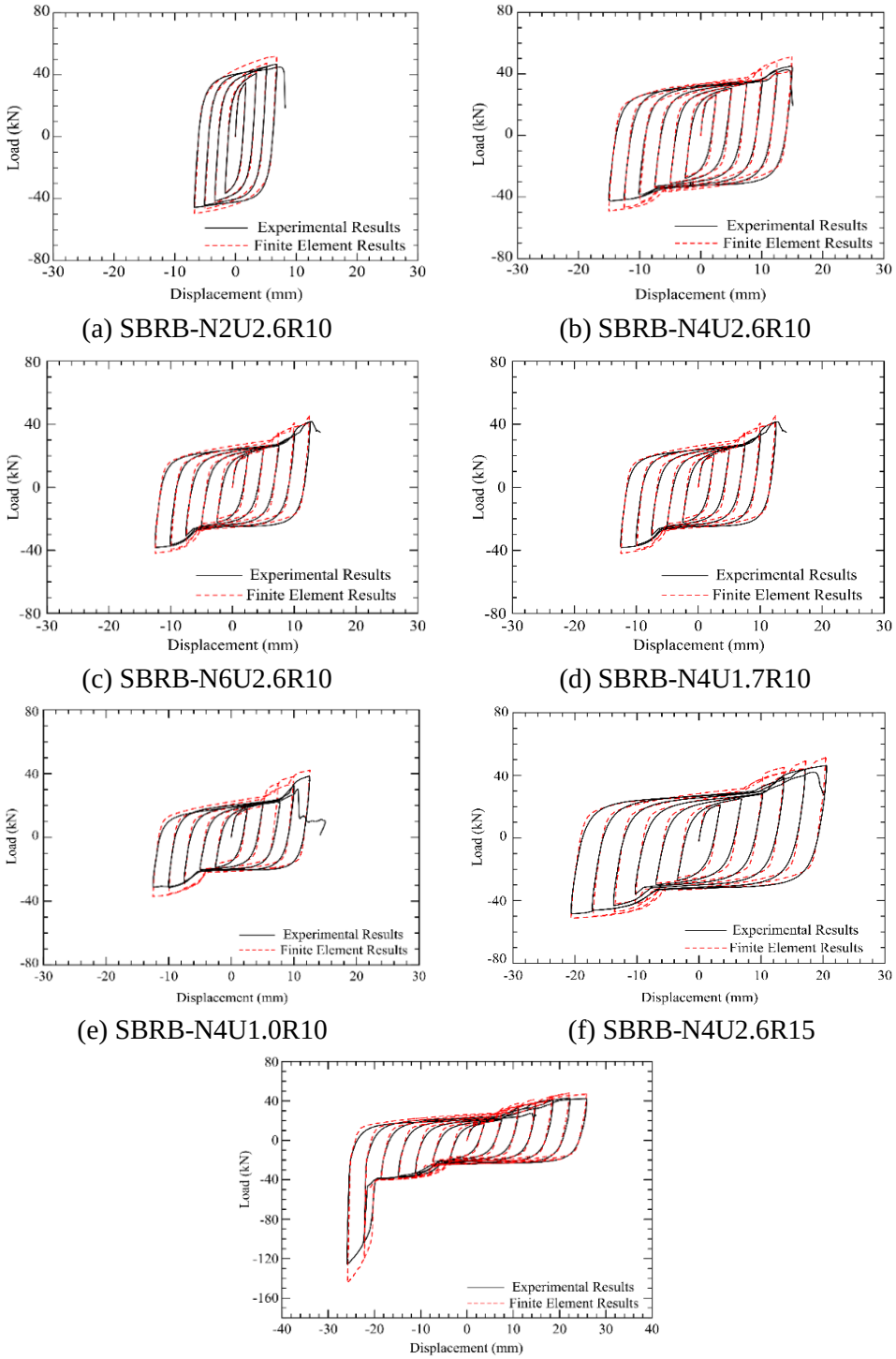

(a) SBRB-N2U2.6R10 (b) SBRB-N4U2.6R10

(c) SBRB-N6U2.6R10 (d) SBRB-N4U1.7R10

(e) SBRB-N4U1.0R10 (f) SBRB-N4U2.6R15

(g) SBRB-N4U2.6R20

Fig. 13 – Hysteretic curves of test and FE results

6. Conclusions

This paper describes a type of shear BRB. Seismic performance of the proposed SBRBs depends on the core plate design details. It was found that the cumulative average plastic strain can achieve up to 92.9% under the

loading history of this study. This value is much larger than those of the previously proposed steel slit dampers and conventional BRBs. Stiffness and strength of the proposed SBRB is uncoupled. Formulae evaluating the yield strength, ultimate strength and initial stiffness of the proposed SBRB can evaluate the experimental results with acceptable accuracy. In addition, the deformation capacity, strength and stiffness of the proposed SBRBs can be easily adjusted by designers. According to FE results, symmetric load-displacement curves under cyclic loading was well simulated and compared well with the experimental ones.

7. Acknowledgements

This study is supported by National Key R&D Program of China (2017YFC0703600) and grants from the Advanced Research Center for Natural Disaster Risk Reduction, Meijo University. The support from the Fundamental Research Funds for the Central Universities is appreciated.

8. References

[1] Skinner RI, Tyler RG, Heine AJ, et al (1980): Hysteretic dampers for the protection of structures from earthquakes. *Bulletin of the New Zealand National Society for Earthquake Engineering*, 13 (1), 22-36

[2] Tsai KC, Hsiao PC (2008): Pseudo dynamic test of a full scale CFT/BRB frame—Part II: Seismic performance of buckling restrained braces and connections. *Earthquake Engineering & Structural Dynamics*, 37 (7), 1099-1115.

[3] Panian L, Bucci N., Janhunen B (2015): Improving the Seismic Performance of Existing Buildings and Other Structures 2015. *ASCE Publications*, pp. 632-643.

[4] Andrews BM, Fahnestock LA, Song J (2009): Ductility capacity models for buckling-restrained braces. *Journal of Constructional Steel Research*, 65 (8-9), 1712-1720.

[5] Tremblay R, Bolduc P, Neville R, et al (2006): Seismic testing and performance of buckling-restrained bracing systems. *Canadian Journal of Civil Engineering* 33 (2), 183-198.

[6] Chou CC, Chen SY (2010): Subassemblage tests and finite element analyses of sandwiched buckling-restrained braces. *Engineering structures*, 32 (8), 2108-2121.

[7] Takeuchi T, Hajjar JF, Matsui R, et al (2012): Effect of local buckling core plate restraint in buckling restrained braces. *Engineering Structures*, 44, 304-311.

[8] Piedrafita D, Cahis X, Simon E, et al (2013): A new modular buckling restrained brace for seismic resistant buildings. *Engineering structures*, 56, 1967-1975.

[9] Piedrafita D, Maimi P, Cahis X (2015): A constitutive model for a novel modular all-steel buckling restrained brace. *Engineering Structures*, 100, 326-331.

[10] Jia LJ, Ge H, Xiang P, et al (2018): Seismic performance of fish-bone shaped buckling-restrained braces with controlled damage process. *Engineering Structures*, 169, 141-153.

[11] Jia LJ, Dong Y, Ge H, et al (2019): Experimental study on high-performance buckling-restrained braces with perforated core plates. *International Journal of Structural Stability and Dynamics*, 19, 1940004.

[12] Piedrafita D, Cahis X, Simon E, et al (2015): A new perforated core buckling restrained brace. *Engineering Structures*, 85, 118-126.

[13] Cahís X, Simon E, Piedrafita D, et al (2018): Core behavior and low-cycle fatigue estimation of the Perforated Core Buckling-Restrained Brace. *Engineering Structures*, 174, 126-138.

[14] Jia LJ, Ge H, Maruyama R, et al (2017): Development of a novel high-performance all-steel fish-bone shaped

buckling-restrained brace. *Engineering Structures*, 138, 105-119.

[15] Karavasilis TL, Kerawala S, Hale E (2012): Hysteretic model for steel energy dissipation devices and evaluation of a minimal-damage seismic design approach for steel buildings. *Journal of Constructional Steel Research*, 70, 358-367.

[16] Benavent-Climent A (2010): A brace-type seismic damper based on yielding the walls of hollow structural sections. *Engineering Structures*, 32 (4), 1113-1122.

[17] Jia LJ, Ikai T, Shinohara K, et al (2016): Ductile crack initiation and propagation of structural steels under cyclic combined shear and normal stress loading. *Construction and Building Materials*, 112, 69-83.

